Published in final edited form as:
Cancer Res. 2013 March 1; 73(5): 1481–1490. doi:10.1158/0008-5472.CAN-12-3429.

Acute and fractionated irradiation differentially modulate glioma stem cell division kinetics

Xuefeng Gao[1], **J. Tyson McDonald**[1], **Lynn Hlatky**[1], and **Heiko Enderling**[1,*]

[1]Center of Cancer Systems Biology, Steward Research Institute, St. Elizabeth's Medical Center, Tufts University School of Medicine, Boston, Massachusetts, USA

Abstract

Glioblastoma multiforme (GBM) is one of the most aggressive human malignancies with a poor patient prognosis. Ionizing radiation (IR) either alone or adjuvant after surgery is part of standard treatment for GBM but remains primarily non-curative. The mechanisms underlying tumor radioresistance are manifold and, in part, accredited to a special subpopulation of tumorigenic cells. The so-called glioma stem cells (GSCs) are bestowed with the exclusive ability to self-renew and repopulate the tumor, and have been reported to be less sensitive to radiation-induced damage through preferential activation of DNA damage checkpoint responses and increased capacity for DNA damage repair. During each fraction of radiation, non-stem cancer cells (CCs) die and GSCs become enriched and potentially increase in number, which may lead to accelerated repopulation. We propose a cellular Potts model (CPM) that simulates the kinetics of GSCs and CCs in glioblastoma growth and radiation response. We parameterize and validate this model with experimental data of the U87-MG human glioblastoma cell line. Simulations are performed to estimate GSC symmetric and asymmetric division rates and explore potential mechanisms for increased GSC fractions after irradiation. Simulations reveal that, in addition to their higher radioresistance, a shift from asymmetric to symmetric division or a fast cycle of GSCs following fractionated radiation treatment is required to yield results that match experimental observations. We hypothesize a constitutive activation of stem cell division kinetics signaling pathways during fractionated treatment, which contributes to the frequently observed accelerated repopulation after therapeutic irradiation.

Keywords

Cellular Potts model; glioma stem cells; CD133; fractionated irradiation; acute irradiation

Major findings

The calibrated Cellular Potts model reproduces experimentally observed *in vitro* and *in vivo* ratios of Glioma Stem Cells (GSCs) in the U87-MG cell line when the frequency of GSC symmetric division events is 35%. The model verifies acute and fractionated irradiation yield enrichment in GSCs due to their reduced radiosensitivity. GSC radioresistance alone, however, while reproducing the 4-fold enrichment in GSCs after acute irradiation, is insufficient to yield the 6-fold enrichment after fractionated irradiation with equal total dose. An additional prolonged increase in GSC symmetric division events or a significantly

[*]Corresponding author: Heiko Enderling, Center of Cancer Systems Biology, Steward Research Institute, St. Elizabeth's Medical Center, Tufts University School of Medicine, 736 Cambridge Street, CBR-115D, Boston, MA 02135, USA, Phone: 617.779.6537, Fax: 617.562.7142, heiko.enderling@tufts.edu.

No potential conflicts of interest are disclosed.

shortened GSC cell cycle after repeated exposure is required to reproduce experimentally observed GSC ratios after fractionated irradiation.

Quick guide to equations and assumptions

We use a Cellular Potts model (CPM) (1,2) to simulate tumor development and response to irradiation. Cells behavior is determined by intrinsic parameters and interaction with adjacent cells, dependent on population-level changes in effective energy E (i.e. Hamiltonian function), which determines cell structure, motility, adhesion and response to extrinsic signals:

$$E=\overbrace{\sum_{\vec{i},\vec{j}\ neighbor} J\left(\tau\left(\sigma\left(\vec{i}\right)\right),\tau\left(\sigma\left(\vec{j}\right)\right)\right)\left(1-\delta\left(\sigma\left(\vec{i}\right),\sigma\left(\vec{j}\right)\right)\right)}^{\text{boundary energy}} + \overbrace{\sum_{\sigma}\lambda_{\text{surface}}(\sigma)\left(v(\sigma)-V_{\text{target}}(\sigma)\right)^2}^{\text{volume constraint energy}} + \overbrace{\sum_{\sigma}\lambda_{\text{surface}}(\sigma)\left(s(\sigma)-S_{\text{target}}(\sigma)\right)^2}^{\text{surface area constraint energy}} \quad (1)$$

where $\vec{i}=(x_i,y_i)$ and $\vec{j}=(x_j,y_j)$ denote neighboring lattice sites, $\sigma(\vec{i})$ denotes the cell at lattice site i, and $J(\tau(\sigma(\vec{i})),\ \tau(\sigma(\vec{j})))$ denotes the contact energy per unit area between cells at neighboring lattice sites. $v(\sigma)$ and $s(\sigma)$ are the volume (total number of pixels in the cell) and surface area which are constrained close to the target volume V_{target} and surface area S_{target} respectively; $\lambda_{\text{volume}}(\sigma)$ and $\lambda_{\text{surface}}(\sigma)$ denote the inverse volume compressibility and inverse membrane compressibility of the cell; and δ is the Kronecker delta with

$$\delta\left(\sigma\left(\vec{i}\right),\sigma\left(\vec{j}\right)\right)=\begin{cases}0, & \text{if } \sigma\left(\vec{i}\right)\neq\sigma\left(\vec{j}\right)\\ 1, & \text{if } \sigma\left(\vec{i}\right)=\sigma\left(\vec{j}\right).\end{cases}$$

The cell lattice evolves through attempts by cells to extend their boundaries into neighboring cells' lattice sites, displacing the neighboring cells that currently occupy those sites. For each index-copy attempt, we randomly select a cell boundary pixel (source) and attempt to displace a randomly chosen neighboring cell pixel (target). The effective energy change, ΔE, is calculated by assuming the source cell displaces the target cell at that pixel. If ΔE is negative (i.e., the change is energetically favorable), the index-copy attempt is accepted. If ΔE is positive, the index-copy attempt is accepted with probability (i.e. Boltzmann acceptance function):

$$P=e^{-\Delta E/T_m} \quad (2)$$

where T_m determines the amplitude of cell membrane fluctuations (equivalent to effective cell motility). These cell rearrangement dynamics involve utilizing relaxational Monte-Carlo-Boltzmann-Metropolis dynamics (3,4). On an N sites lattice, N displacement attempts are made in each Monte Carlo Step (MCS). The translation of experimental time into MCS depends on the average ratio of $\Delta E/T_m$ (2). Simulations are performed in the open-source CompuCell3D simulation environment (2) on a 4000×4000 square lattice with periodic boundary conditions and T_m=50 (c.f., Eq. 2).

Assumptions

Glioblastoma are heterogeneous with subpopulations of glioma stem cells (GSCs) and non-stem cancer cells (CC). The kinetics and interactions of both populations dictate dynamics of the population as a whole.

Basic cell kinetics

Cells are considered individual entities with a cell cycle (with length T_C) and a limited proliferation capacity ρ=[0, ρ_{max}]. For GSCs, ρ_{max}=∞. At each cell division, GSCs undergo symmetric division with probability p_s to produce two GSCs with identical features, or with probability $1-p_s$ asymmetric division to produce a GSC and a CC with limited proliferation capacity ρ_{max}. The proliferation capacity ρ is decremented at each CC division and inherited by both daughter CCs. CCs die when a proliferation attempt yields ρ<0 (Figure 1). To model proliferation, cell target volume $V_{\text{target}}(\sigma)$ is increased with growth rate k until the actual cell volume $v(\sigma)$ is doubled. If the local environment is not favorable for cell growth and cells cannot reach their target volume (that is, the effective energy change, ΔE for a cell to increase in size is so large that the Boltzmann acceptance probability P (c.f., Eq. 2) becomes infinitesimal), cells are considered growth arrested, or quiescent.

Radiation response model

After exposure to irradiation cells become arrested in the cell cycle and attempt to repair radiation-induced DNA damage (5). The probability of successful repair and thus cell survival after application of dose d is modeled using the established linear-quadratic (LQ) model:

$$S = e^{-\xi\lambda(\alpha d+\beta d^2)} \quad (3)$$

where αd describes cell killing due to a single event, and βd^2 describes cell killing after combination of two independent, potentially repairable events, with α and β being cell-specific radiosensitivity parameters (6). We introduce ξ and λ as radiation protection factors for quiescent cells and GSCs, respectively. The basic LQ model has been extended to take into account the effects of inter-fraction tumor repopulation (6). Alternatively, the LQ model can be applied repeatedly as independent events at discrete time intervals if inter-fraction population dynamics are simulated by a tumor growth model (7,8). We assume the cells that are fated to die undergo cell death at the next division attempt, which is achieved by setting the proliferation capacity of a hit cell to ρ=0.

Introduction

GBM are among the most lethal primary human malignancies, possessing rapid growth, high invasiveness and treatment resistance. Standard treatment for GBM comprises surgical resection of the gross tumor mass followed by radiotherapy of 60 Gy in 30–33 fractions of 1.8–2 Gy (9). The prognosis for patients with GBM remains poor because of refractory response to radiation and other treatments (10,11). Therapeutic failure is due, in part, to tumor cell heterogeneity derived from both genetic and epigenetic sources (12). GBM frequently recur after treatment with ionizing irradiation (IR) (13), indicating survival of tumorigenic cells. It has been shown that only a subpopulation of cells – the so-called glioma stem cells (GSCs) – are able to initiate brain tumors in a mouse model (14–16). Studies from our group and other laboratories have demonstrated that the number of cancer colonies correlates with the frequency of cancer stem cells (17,18). The population of GSCs has been shown to be highly resistant to IR due to more efficient DNA damage response mechanisms and environmental survival cues (11,19–21). By detecting the expression of

CD133 (Prominin-1), a pivotal marker of putative GSC, the percentage of GSCs as well as their population size was found to be increased after radiation exposure (11,21,22). Importantly, irradiation did not induce CD133 expression in $CD133^-$ cells, confirming that increase in $CD133^+$ cells is due to proliferation of the original $CD133^+$ subpopulation. Surviving GSCs are able to initiate secondary tumors with enhanced aggressiveness and decreased latencies relative to untreated tumors (11,23). The survival and increase of the GSC population during radiation therapy may be a leading cause of accelerated and more aggressive GBM recurrence after radiation therapy.

In the present study, we found that resistance of GSCs to IR alone is insufficient to explain the experimentally observed increased GSC ratios after fractionated radiation treatment. We show that an additional radiation-induced shift in GSC division in favor of symmetric division or a faster cycling time reproduces the reported *in vitro* and *in vivo* enrichment of GSCs (22). Based on our previous studies (8,17,24,25), we develop a cellular Potts model (CPM) that simulates cancer stem cell-driven GBM growth and radiation response. In particular, this model estimates symmetric and asymmetric GSC division rates before and after irradiation, and simulates the growth dynamics of the irradiated GBM population with and without irradiation-induced constitutive changes in GSC division dynamics.

Materials and Methods

Cell Culture

The U87-MG cell line was obtained from American Type Culture Collection (ATCC, Bethesda, MD, USA) where cell line authentication and species identification was performed. Cells were grown in Minimum Essential Medium (MEM, Invitrogen Life Technologies, Grand Island, NY) supplemented with 10% fetal bovine serum (FBS, Lonza, Hopkinton, MA) and maintained at 37°C with 5% CO_2 in humidified air. Time-lapse video microscopy was used to monitor cell behavior. Images were taken every 15 minutes, by using a digital camera (Photometric Coolsnap HQ2 CCD) coupled to an inverted microscope. We used CellTrack (26), an open source software, for cell tracking and motility analysis to estimate cell proliferation and migration rates.

For clonogenic survival assays, single cell suspensions were irradiated with the Gammacell 40 irradiator (MDS Nordion, Inc., Ottawa, ON, Canada) with doses ranging from 0–16 Gy at 0.48 Gy per minute. Irradiated cells were plated in 10 cm dishes at low density. Cells were fixed with 70% ethanol, stained with 0.2% crystal violet 14 days after irradiation. Cell colonies of 50 cells or more were scored.

Simulation Process

Cellular kinetics are simulated through the following steps (Figure 1):

1. Increase the target volume of cell σ with fixed rate k.
2. If the volume of cell σ is doubled ($v(\sigma) \geq 2v_0$) cell division is attempted.
    a. If cell σ is a GSC, it divides symmetrically with probability p_s to produce two GSCs, or asymmetrically with probability $1-p_s$ to produce a GSC and a CC with limited proliferation potential ρ_{max} (see next section).
    b. If cell σ is a CC, both daughter CCs inherit a decremented proliferation capacity $\rho-1$.
3. If the proliferation capacity of cell σ is exhausted ($\rho=0$), the death of cell σ is invoked by setting $V_{\text{target}}(\sigma)=0$.

4. Cell σ is labeled as currently quiescent when no increase in cell volume $v(\sigma)$ has occurred for consecutive simulated t=6 hrs (180 MCS).
5. If a cell σ is irradiated, the cell gets arrested in its cell cycle for a period of time T_a.
6. If a cell σ is unrepaired when re-entering the cycle (calculated by Eq. (3)), cell death is evoked by setting proliferation capacity ρ=0.

Parameterization

We set the initial size of a cancer cell in the cellular Potts model (CPM) to v_0=4×4 pixels. We estimated the average diameter of U87-MG cell, r, *in vitro* at approximately 10 μm (n=20). Using these measurements, 1 pixel equals 2.5 μm×2.5 μm. The average migration speed of U87-MG cells, v, *in vitro* is 23.4 μm hr^{-1} (n=24, Figure 2A), which is in good agreement with the literature (27,28). The average replacement of cells in CPM is approximately 0.31 pixels MCS^{-1} (Figure 2B). Equating experimental and simulated cell migration speeds implies that 30 MCS approximate 1 hr. By tracking two consecutive mitotic events of individual U87-MG cells we obtained the cell cycle length to be T_c=25 hrs (n=22). Therefore, the growth rate of *in silico* cells is $k = (V_{\text{target}} - v_0)/T_c$ =0.0213 pixel MCS^{-1}, where $V_{\text{target}} = 2v_0$ represents the doubling volume of cancer cells. The proliferation potential of CC is set to ρ_{max} = 10 which has previously been shown to enable fast tumor growth (17).

Radiation-induced cell cycle arrest of U87-MG cells is observable through a decreased mitotic index immediately after irradiation that returns to control levels after 16 hrs (5). We assign a cell cycle arrest time $0 \leq T_a \leq 16$ hrs for each cell from a uniform distribution. Using clonogenic assays for long-term cell survival of U87-MG cells after single doses of radiation ranging from 0–16 Gy, we derived for sensitivity parameters in the LQ model (Eq. 3) the unconstrained best-fit values of α=0.3859 and β=0.01148 (Figure 3). Radioresistance of quiescent cells is a major determinant for treatment success (29), and the spatial distribution of proliferating cells and their killing by radiation plays a crucial role in the redistribution of quiescent cells into the cell cycle (8). For radiosensitive proliferating cells we assume ξ=1, and a reduced sensitivity of ξ=0.5 is assumed for non-cycling quiescent cells (30,31).

To match the reported increase in GSC fraction after different doses of irradiation (22), survival probabilities above 100% are required, which implies that different α and β values for GSC alone are insufficient to explain the reported data. Nevertheless, GSC radiation response parameters need to be reliably identified in the future. From the dose response survival curves (Figure 3) we estimate the GSC radiation protection factor λ_{GSC}=0.1376 by applying 4.5-fold lower apoptosis rate than CCs (λ_{CC} =1) at 3 Gy radiation as reported (11). Model parameters with their values are listed in Table 1.

Results

Tumor population growth

To compare *in silico* tumor population formation with observed *in vitro* morphologies we place a GSC in the center of the computational lattice and monitor tumor growth for 15 days. The seeded cell performs a random walk and gives rise to two daughter cells that subsequently repeat the aforementioned dynamics. An initially sparse collection of cells forms an *in silico* tumor population (Figure 2D) comparable to *in vitro* U87-MG growth (Figure 2C).

Estimation of GSCs symmetric division rate

The fraction of U87 $CD133^+$ cells *in vitro* and *in vivo* has recently been estimated to be 1.8–3.0% (33), which is comparable to 2.51 ± 2.12% GSCs reported in primary GBM specimens. The frequency of GSCs depends pivotally on the frequency of symmetric GSC division events (p_s in our model) to expand the stem cell pool. To estimate the symmetric division rate of GSCs we simulate tumor growth with varying p_s values. By comparing the frequency of GSCs in *in silico* tumors of 10^5 cells with the reported fraction of $CD133^+$ cells we estimated the symmetric division rate to be 35–45% (p_s=0.35–0.45) for the U87-MG glioblastoma cell line (Figure S1). Taking the lower boundary, i.e. p_s=0.35, we simulate the growth of five tumors from one GSC to a population of ~10^5 cells with average 1.81% GSCs (n=5) (Figure 4).

Enrichment of GSCs

We simulate continuing tumor growth either without (control) or with exposure to IR, and compare GSC fractions and tumor progression rates. Utilizing available data in the literature we simulate single-dose irradiation with 6 Gy. At 48 hrs after irradiation, the simulated percentage of GSCs is 7.4%, approximately 4.1-fold enrichment relative to the untreated control (1.81%, c.f. Figure 4A), reproducing the increased ratios of GSCs reported in the literature (3–5 fold) (11,22). The observed enrichment is due to (*i*) a larger fraction CCs being killed by IR, and (*ii*) GSCs re-entering the proliferation cycle.

Surprisingly, GSC enrichment to 10.33% after fractionated radiation of 3×2 Gy as reported experimentally (22) was not observed in the CPM, even if increased damage repair in GSCs (11) yields no GSC cell cycle arrest and immediate advancement in the cell cycle (Figure 4A). This disparity indicates that the increase in the proportion of GSCs was not only caused by selection of a radioresistant subpopulation but also an increase in GSC population. Therefore, we hypothesize that repeated exposure to radiation might alter the division kinetics of GSCs. The underlying mechanisms might be comparable to activated signaling pathways such as Sonic Hedgehog (SHh), Notch, Wnt and epidermal growth factor receptor (EGFR), that enable the expansion of the somatic stem cell pool through increased symmetric division during normal development and wound healing (34). Radiation has furthermore been shown to activate the AKT/cyclin D1/Cdk4 pathway in human glioblastoma cells (35), which yields a significantly shorter cell cycle time of 15–16 hrs in human embryonic stem cells compared to somatic cells due to an abbreviated G1 phase (36). As single dose IR of 2 Gy did not cause a significant change in the population of $CD133^+$ cells *in vivo* (22), it is conceivable that either symmetric division probability p_s or GSC growth rate k increases during repeated exposure to IR or, as considered herein, constitutively after the second fraction of radiation. Applying a constitutive *(i)* increase of p_s=0.75 or *(ii)* decrease of T_c=12 hrs (and therefore an increase in growth rate k per time unit) yields GSC fractions after 48 hrs in best agreement with the experimental observation (22) (Figure 4A). A similarly good fit was observed for *(iii)* the combination of partial modulation of both mechanisms (p_s=0.55, T_c=18.5 hrs; both mechanisms modulated by half of the estimated difference when altered individually) (Figure 4A).

Accelerated Tumor Repopulation

Simulated tumors of 10^5 cells treated with fractionated 3×2 Gy IR reach pre-treatment size 6 days after treatment start (3 days after final dose) (Figure 4B), and 3 weeks after treatment start the average mass of irradiated tumors exceeds that of untreated control tumors. While control tumors took 14 days to double their cell number (to 2×10^5 cells), tumors treated with fractionated IR doubled in 10 days. The overall tumor population growth rates (not to be confused with cell growth rate k) after treatment with fractionated IR for all hypotheses (*i-iii*) are unanimously greater than 0.05 (Table 2), while untreated control tumors grow at a

rate of 0.0389, which is in excellent agreement with previous untreated glioblastoma growth rate estimations (37,38). Tumor composition 30 days after treatment began, however, is remarkably different for tumors after fractionated irradiation following the different hypotheses discussed above. While tumors with a shortened T_C=12 hrs (hypothesis (*ii*)) have the fewest stem cells, their total cell number is the highest due to frequent production of CCs. Tumors formed by GSCs with largest p_s=0.75 (hypothsis (*i*)) contain the largest number of GSCs, but the least overall total number of cells due to the longer cell cycle compared hypotheses (*ii*) and (*iii*) (Figure 4B,C).

Exposure to single 6 Gy IR also yields tumors of pre-treatment size within 7 days (Figure 4B,C) but the modest increase in GSC numbers does not yield an apparent accelerated growth in the short time frame observed. The tumor population growth rate of 0.0445, however, is slightly larger than that of the untreated control, and the thus treated tumor is expected to outgrow the untreated tumor 49 days after treatment. The simulation statistics are summarized in Table 2.

Discussion

We have presented a CPM of GSC and CC kinetics in glioblastoma growth and response to IR. The study aimed to identify cancer stem cell division modes that generate observed frequencies of cancer stem cells in GBM, as well as the role of GSCs in glioblastoma response to IR and subsequent accelerated repopulation. The key cell kinetics parameters in the model were calibrated using experimental data obtained in our laboratory as well as from the literature, yielding simulations of population growth that are in good agreement with experimental results. We obtained the best agreement with reported fractions of GSCs if symmetric division occurs in 35–45% of mitotic GSC events. Whilst these division probabilities reproduce experimentally observed enrichment ratios after single-dose irradiation, our simulations reveal that such frequencies are insufficient to reproduce the 6-fold enrichment observed after exposure to identical dose delivered in smaller fractions.

We hypothesized that fractionated radiation increases activation of GSC signaling pathways such as AKT/cyclin D1/Cdk4, SHh, Notch, Wnt and EGFR, which have been shown to orchestrate stem cell survival, self-renewal, proliferation, and differentiation during normal tissue development and repair (34) (Figure 5). While these pathways that are tightly regulated in normal tissue, it is conceivable that their regulation is aberrant in tumors (Figure 5). Recently, Lathia and colleagues showed that GSC division mode is regulated by growth factors including epidermal growth factor (EGF) and fibroblast growth factor (FGF) (39). EGF-mediated signaling pathways have been shown to contribute to increased migration, survival, proliferation and self-renewal capacity (40), and to maintain the stemness of GSCs with enhanced malignant phenotypes (41). SHh-Gli signaling is required for self-renewal and tumorigenic potential of GSCs, and its inhibition is able to prevent GSCs proliferation (42). Notch signaling is highly involved in regulating self-renewal and expansion of many different types of normal and cancer stem cells (43). Inhibition of Notch signaling in GSCs (e.g., by γ-secretase inhibitor) attenuates the formation of neurosphere-like colonies, increases neuronal differentiation, reduces $CD133^+$ cell fraction *in vitro*, and decreases tumorigenicity *in vivo* (44), whilst its overexpression has been linked to GSC radioresistance (45) much like Wnt signaling (46–48). Particularly, Notch2 was markedly upregulated in glioma cells treated with fractionated radiation comparing to single-dose radiation (22) lending further support to our hypothesis. Increased activation of Notch-1 following fractionated radiation was also found in breast cancer stem cells conceiving a possible mechanism for the accelerated repopulation of breast tumors following radiotherapy (49).

Model simulations show that either an increased symmetric division rate or a faster cell cycle of GSCs after repeated exposure to radiation is sufficient to reproduce the elevated enrichment observed experimentally. Frequencies of symmetric GSC division even larger than the herein estimated 75% have been reported recently if exposed to the right milieu of growth factors (39), and aforementioned literature suggests that fractionated irradiation is capable of creating such environment. Observations or references to the alternative hypothesis of a post-irradiation cell cycle in glioma cells as short as 12 hrs, however, are unbeknownst to the authors. It is, nevertheless, conceivable that the increased activation of stem cell division kinetics signaling pathways as discussed above partially modulates both cell cycle progression as well as symmetric division of GSCs. The simulated example with p_s=55% and T_c=18.5 hrs (both mechanisms modulated by half of the estimated difference when altered individually) reproduces the experimental data similarly well with biologically relevant parameter values. Increase in GSC symmetric division rate appears to be the dominant mechanism for increasing the GSC pool, which is in line with previous calculations that regulation of self-renewal is essential for efficient repopulation in the healthy hematopoietic system (50). Future experiments will need to identify which of the discussed hypotheses is prevalent after fractionated irradiation of glioblastoma cells.

Taken together, the presented study reveals that sub-lethal perturbation of a primary GBM selects for and increases the more aggressive subpopulation of GSCs, yielding accelerated repopulation, fast recurrence and worsens prognosis, as previously hypothesized (11,23). If GSCs survive irradiation, recurring tumors show increased population growth rates. Consequently, pre-treatment tumor sizes will be acquired relatively shortly after irradiation with inadequate dose, and inevitably such treated tumors will outgrow untreated control. Whilst the diffusive nature of GBM is the major cause for tumor recurrence, fractionated irradiation-induced increase in GSC self-renewal capacity and/or accelerated cell cycle progression are conceivable as general mechanisms contributing to tumor resistance and accelerated repopulation after apparently adequate radiation treatment.

For computational convenience we focused in our study on early microscopic tumors. Tumors smaller than diffusion-limited size (approximately 1 mm in diameter, 10^6 cells) are fully oxygenated (51), and therefore hypoxia can be ignored in the presented model. It is of note, however, that self-metastatic tumor growth is self-similar and population composition at smaller sizes is representative for later tumors (17,52). For the applicability of the treatment model we might argue that such microscopic tumors exist in the target area of radiation. GBM are highly infiltrative, and while surgery removes the bulk of the tumor, an appreciable number of cancer cells and microscopic foci have diffused beyond surgical margin throughout the brain (53).

We used *in vitro* data to parameterize radiosensitivity parameters of the linear-quadratic model (Eq. 3). The obtained α and β values are an order of magnitude larger than estimated by Rockne and colleagues (54) to match clinical response of primary GBM. By scaling the radiosensitivity of quiescent cells (ξ) as well as GSCs (λ), however, the linear sensitivity parameter α of the overall population matches their estimated parameters from clinical response data (54).

The only parameter in the presented model that we are unable to estimate (and to our knowledge has not been reported in the literature) is the proliferation capacity ρ_{max} of CC. We assumed ρ_{max}=10 based on previous simulation results that revealed aggressive tumor progression for this parameter value (17). This parameter, however, plays a pivotal role in modulating the frequency of cancer stem cells in solid tumors (52). Therefore, the estimated GSC symmetric division rate of 35–45% to yield 1.8–3.0% of GSC in the total tumor population is only an estimate that is closely linked to the chosen CC proliferation capacity.

Further experimental work into identifying the proliferation capacity of CC is required to confidently derive GSC division modes pre- and post therapeutic intervention. Furthermore, our studies were carried out on the U87-MG glioblastoma cell line that was reported in the literature (22). This cell line has limited capability to recapitulate the *in vivo* biology of human glioblastoma, and further validation on primary GSCs are required before profound conclusions for treatment planning can be drawn.

Supplementary Material

Refer to Web version on PubMed Central for supplementary material.

Acknowledgments

Grant Support

This project was supported by the National Cancer Institute under Award Number U54CA149233 (to L. H.). The content is solely the responsibility of the authors and does not necessarily represent the official views of the National Cancer Institute or the National Institutes of Health.

References

1. Glazier J, Graner F. Simulation of the differential adhesion driven rearrangement of biological cells. Phys Rev E Stat Phys Plasmas Fluids Relat Interdiscip Topics. 1993; 47(3):2128–54. [PubMed: 9960234]
2. Swat MH, Hester SD, Balter AI, Heiland RW, Zaitlen BL, Glazier JA. Multicell simulations of development and disease using the CompuCell3D simulation environment. Methods Mol Biol. 2009; 500:361–428. [PubMed: 19399437]
3. Metropolis N, Rosenbluth AW, Rosenbluth MN, Teller AH, Teller E. Equation of State Calculations by Fast Computing Machines. J Chem Phys. 1953; 21(6):1087.
4. Cipra B. An introduction to the Ising model. The American Mathematical Monthly. 1987; 94(10): 937–59.
5. McCord AM, Jamal M, Williams ES, Camphausen K, Tofilon PJ. CD133+ glioblastoma stem-like cells are radiosensitive with a defective DNA damage response compared with established cell lines. Clin Cancer Res. 2009; 15(16):5145–53. [PubMed: 19671863]
6. Brenner DJ, Hlatky L, Hahnfeldt PJ, Hall EJ, Sachs RK. A convenient extension of the linear-quadratic model to include redistribution and reoxygenation. Int J Radiat Oncol Biol Phys. 1995; 32(2):379–90. [PubMed: 7751180]
7. Enderling H, Chaplain MAJ, Anderson ARA, Vaidya JS. A mathematical model of breast cancer development, local treatment and recurrence. J Theor Biol. 2007; 246(2):245–59. [PubMed: 17289081]
8. Enderling H, Park D, Hlatky L, Hahnfeldt P. The Importance of Spatial Distribution of Stemness and Proliferation State in Determining Tumor Radioresponse. Math Model Nat Phenom. 2009; 4(3): 117–33.
9. Stupp R, Roila F. ESMO Guidelines Working Group. Malignant glioma: ESMO clinical recommendations for diagnosis, treatment and follow-up. Ann of Oncol. 2009; (Suppl 4):126–8. [PubMed: 19454432]
10. Legler JM, Ries LAG, Smith MA, Warren JL, Heineman EF, Kaplan RS, et al. Brain and Other Central Nervous System Cancers: Recent Trends in Incidence and Mortality. J Natl Cancer Inst. 1999; 91(16):1382–90. [PubMed: 10451443]
11. Bao S, Wu Q, Mclendon RE, Hao Y, Shi Q, Hjelmeland AB, et al. Glioma stem cells promote radioresistance by preferential activation of the DNA damage response. Nature. 2006; 444(7120): 756–60. [PubMed: 17051156]
12. Anderson K, Lutz C, van Delft FW, Bateman CM, Guo Y, Colman SM, et al. Genetic variegation of clonal architecture and propagating cells in leukaemia. Nature. 2011; 469(7330):356–61. [PubMed: 21160474]

13. Garden AS, Maor MH, Yung WK, Bruner JM, Woo SY, Moser RP, et al. Outcome and patterns of failure following limited-volume irradiation for malignant astrocytomas. Radiother Oncol. 1991; 20(2):99–110. [PubMed: 1851573]
14. Singh SK, Clarke ID, Terasaki M, Bonn VE, Hawkins C, Squire J, et al. Identification of a cancer stem cell in human brain tumors. Cancer Res. 2003; 63(18):5821–8. [PubMed: 14522905]
15. Singh SK, Clarke ID, Terasaki M, Bonn VE, Hawkins C, Squire J, et al. Identification of a Cancer Stem Cell in Human Brain Tumors. Cancer Res. 2003; 63(18):5821–8. [PubMed: 14522905]
16. Hemmati HD, Nakano I, Lazareff JA, Masterman-Smith M, Geschwind DH, Bronner-Fraser M, et al. Cancerous stem cells can arise from pediatric brain tumors. Proc Natl Acad Sci USA. 2003; 100(25):15178–83. [PubMed: 14645703]
17. Enderling H, Hlatky L, Hahnfeldt P. Migration rules: tumours are conglomerates of self-metastases. Br J Cancer. 2009; 100(12):1917–25. [PubMed: 19455139]
18. Mani SA, Guo W, Liao M-J, Eaton EN, Ayyanan A, Zhou AY, et al. The epithelial-mesenchymal transition generates cells with properties of stem cells. Cell. 2008; 133(4):704–15. [PubMed: 18485877]
19. Hambardzumyan D, Becher OJ, Rosenblum MK, Pandolfi PP, Manova-Todorova K, Holland EC. PI3K pathway regulates survival of cancer stem cells residing in the perivascular niche following radiation in medulloblastoma in vivo. Genes Dev. 2008; 22(4):436–48. [PubMed: 18281460]
20. Kang MK, Hur BI, Ko MH, Kim CH, Cha SH, Kang SK. Potential identity of multi-potential cancer stem-like subpopulation after radiation of cultured brain glioma. BMC Neurosci. 2008; 9:15. [PubMed: 18230189]
21. Tamura K, Aoyagi M, Wakimoto H, Ando N, Nariai T, Yamamoto M, et al. Accumulation of CD133-positive glioma cells after high-dose irradiation by Gamma Knife surgery plus external beam radiation. J Neurosurg. 2010; 113(2):310–8. [PubMed: 20205512]
22. Kim M-J, Kim R-K, Yoon C-H, An S, Hwang S-G, Suh Y, et al. Importance of PKCδ signaling in fractionated-radiation-induced expansion of glioma-initiating cells and resistance to cancer treatment. J Cell Sci. 2011; 124(Pt 18):3084–94. [PubMed: 21878493]
23. Hillen T, Enderling H, Hahnfeldt P. The Tumor Growth Paradox and Immune System-Mediated Selection for Cancer Stem Cells. Bull Math Biol. 201210.1007/s11538-012-9798-x
24. Enderling H, Chaplain MAJ, Hahnfeldt P. Quantitative modeling of tumor dynamics and radiotherapy. Acta Biotheor. 2010; 58(4):341–53. [PubMed: 20658170]
25. Gao X, Tangney M, Tabirca S. A Multiscale Model for Hypoxia-induced Avascular Tumor Growth. In proceeding of 2011 International Conference on Bioscience, Biochemistry and Bioinformatics. 2011; 5:53–8.
26. Sacan A, Ferhatosmanoglu H, Coskun H. CellTrack: an open-source software for cell tracking and motility analysis. Bioinformatics. 2008; 24(14):1647–9. [PubMed: 18511469]
27. Sabari J, Lax D, Connors D, Brotman I, Mindrebo E, Butler C, et al. Fibronectin matrix assembly suppresses dispersal of glioblastoma cells. PLoS ONE. 2011; 6(9):e24810. [PubMed: 21980357]
28. Nakada M, Anderson EM, Demuth T, Nakada S, Reavie LB, Drake KL, et al. The phosphorylation of ephrin-B2 ligand promotes glioma cell migration and invasion. Int J Cancer. 2010; 126(5): 1155–65. [PubMed: 19728339]
29. Withers HR. Four R's of radiotherapy. Adv Radiat Biol. 1975; 5:241–7.
30. Hall, EJ.; Giaccia, AJ. Radiobiology for the radiologist. Lippincott Williams and Wilkins; Philadelphia, Pa, USA: 2006.
31. Potten CS. The cell kinetic mechanism for radiation-induced cellular depletion of epithelial tissue based on hierarchical differences in radiosensitivity. Int J Radiat Biol Relat Stud Phys Chem Med. 1981; 40(2):217–25. [PubMed: 6974149]
32. Norton L. Conceptual and Practical Implications of Breast Tissue Geometry: Toward a More Effective, Less Toxic Therapy. The Oncologist. 2005; 10(6):370–81. [PubMed: 15967831]
33. Ulasov I, Nandi S. Inhibition of Sonic Hedgehog and Notch Pathways Enhances Sensitivity of CD133+ Glioma Stem Cells to Temozolomide Therapy. Mol Med The Feinstein Institute for Medical Research. 2011; 17(1–2):1.
34. Beachy PA, Karhadkar SS, Berman DM. Tissue repair and stem cell renewal in carcinogenesis. Nature. 2004; 432(7015):324–31. [PubMed: 15549094]

35. Shimura T, Noma N, Oikawa T, Ochiai Y, Kakuda S, Kuwahara Y, et al. Activation of the AKT/cyclin D1/Cdk4 survival signaling pathway in radioresistant cancer stem cells. Nat Rev Cancer. 2012; 1(6):e12.
36. Becker KA, Ghule PN, Therrien JA, Lian JB, Stein JL, van Wijnen AJ, et al. Self-renewal of human embryonic stem cells is supported by a shortened G1 cell cycle phase. J Cell Physiol. 2006; 209(3):883–93. [PubMed: 16972248]
37. Harpold HLP, Alvord EC, Swanson KR. The evolution of mathematical modeling of glioma proliferation and invasion. J Neuropathol Exp Neurol. 2007; 66(1):1–9. [PubMed: 17204931]
38. Rockne R, Alvord EC Jr, Rockhill JK, Swanson KR. A mathematical model for brain tumor response to radiation therapy. J Math Biol. 58(4–5):561–78. [PubMed: 18815786]
39. Lathia JD, Hitomi M, Gallagher J, Gadani SP, Adkins J, Vasanji A, et al. Distribution of CD133 reveals glioma stem cells self-renew through symmetric and asymmetric cell divisions. Cell Death Dis. 2011; 2:e200. [PubMed: 21881602]
40. Ayuso-Sacido A, Moliterno JA, Kratovac S, Kapoor GS, O'Rourke DM, Holland EC, et al. Activated EGFR signaling increases proliferation, survival, and migration and blocks neuronal differentiation in post-natal neural stem cells. J Neurooncol. 2009; 97(3):323–37. [PubMed: 19855928]
41. Mazzoleni S, Politi LS, Pala M, Cominelli M, Franzin A, Sergi Sergi L, et al. Epidermal growth factor receptor expression identifies functionally and molecularly distinct tumor-initiating cells in human glioblastoma multiforme and is required for gliomagenesis. Cancer Res. 2010; 70(19): 7500–13. [PubMed: 20858720]
42. Takezaki T, Hide T, Takanaga H, Nakamura H, Kuratsu J-I, Kondo T. Essential role of the Hedgehog signaling pathway in human glioma-initiating cells. Cancer Science. 2011; 102(7): 1306–12. [PubMed: 21453386]
43. Wang Z, Li Y, Banerjee S, Sarkar FH. Emerging role of Notch in stem cells and cancer. Cancer Letters. 2009; 279(1):8–12. [PubMed: 19022563]
44. Fan X, Matsui W, Khaki L, Stearns D, Chun J, Li Y-M, et al. Notch pathway inhibition depletes stem-like cells and blocks engraftment in embryonal brain tumors. Cancer Res. 2006; 66(15): 7445–52. [PubMed: 16885340]
45. Wang J, Wakeman TP, Lathia JD, Hjelmeland AB, Wang X-F, White RR, et al. Notch Promotes Radioresistance of Glioma Stem Cells. Stem Cells. 2009; 28(1):17–28. [PubMed: 19921751]
46. Gupta R, Vyas P, Enver T. Molecular Targeting of Cancer Stem Cells. Cell Stem Cell. 2009; 5(2): 125–6. [PubMed: 19664981]
47. Jin X, Jeon H-Y, Joo KM, Kim J-K, Jin J, Kim SH, et al. Frizzled 4 regulates stemness and invasiveness of migrating glioma cells established by serial intracranial transplantation. Cancer Res. 2011; 71(8):3066–75. [PubMed: 21363911]
48. Kim Y, Kim KH, Lee J, Lee Y-A, Kim M, Lee SJ, et al. Wnt activation is implicated in glioblastoma radioresistance. Lab Invest. 2011; 92(3):466–73. [PubMed: 22083670]
49. Phillips TM, McBride WH, Pajonk F. The Response of CD24−/low/CD44+ Breast Cancer-Initiating Cells to Radiation. J Natl Cancer Inst. 2006; 98(24):1777–85. [PubMed: 17179479]
50. Marciniak-Czochra A, Stiehl T, Ho AD, Jager W, Wagner W. Modeling of Asymmetric Cell Division in Hematopoietic Stem Cells—Regulation of Self-Renewal Is Essential for Efficient Repopulation. Stem Cells and Dev. 2009; 18(3):377–86.
51. Stanley JA, Shipley WU, Steel GG. Influence of tumour size on hypoxic fraction and therapeutic sensitivity of Lewis lung tumour. Br J Cancer. 1977; 36(1):105–13. [PubMed: 889677]
52. Morton CI, Hlatky L, Hahnfeldt P, Enderling H. Non-stem cancer cell kinetics modulate solid tumor progression. Theor Biol Med Model. 2011; 8:48. [PubMed: 22208390]
53. Swanson KR, Alvord EC, Murray JD. Virtual brain tumours (gliomas) enhance the reality of medical imaging and highlight inadequacies of current therapy. Br J Cancer. 2002; 86(1):14–8. [PubMed: 11857005]
54. Rockne R, Rockhill JK, Mrugala M, Spence AM, Kalet I, Hendrickson K, et al. Predicting the efficacy of radiotherapy in individual glioblastoma patients in vivo: a mathematical modeling approach. Phys Med Biol. 2010; 55(12):3271–85. [PubMed: 20484781]

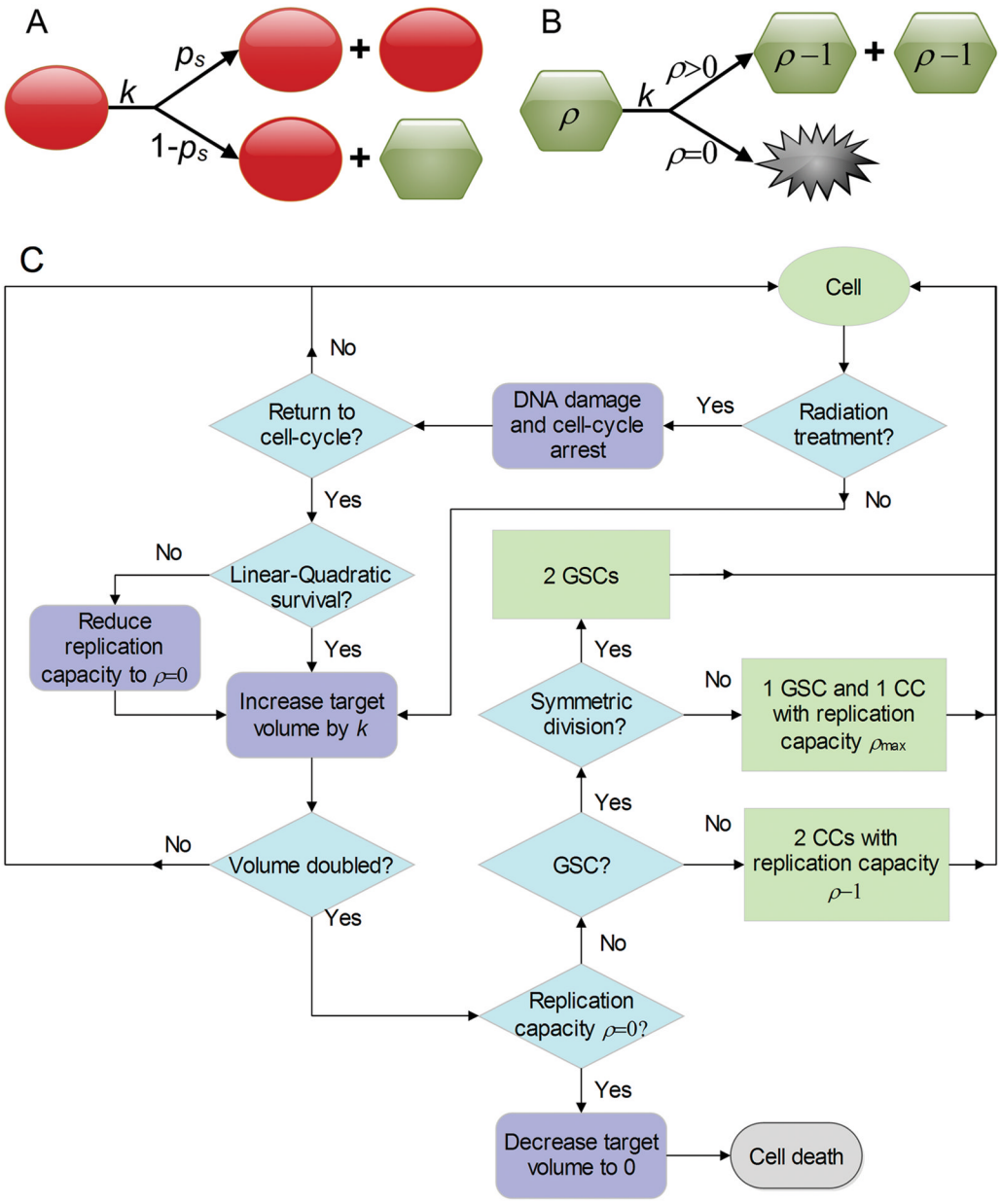

Figure 1.

Schematic of cell division fate model. **(A)** Glioma stem cells (GSC, red circle) divide with rate *k*, either symmetrically with probability p_s or asymmetrically with probability $1-p_s$, where one daughter cell is a non-stem cancer cell (CC, green hexagon) with proliferation potential ρ_{max}. **(B)** Non-stem cancer cells (CC, green hexagon) grow with rate k, and produce two CCs with decremented proliferation potential $\rho-1$ if $\rho>0$, or die if proliferation potential is exhausted ($\rho=0$). **(C)** Flowchart of simulation process.

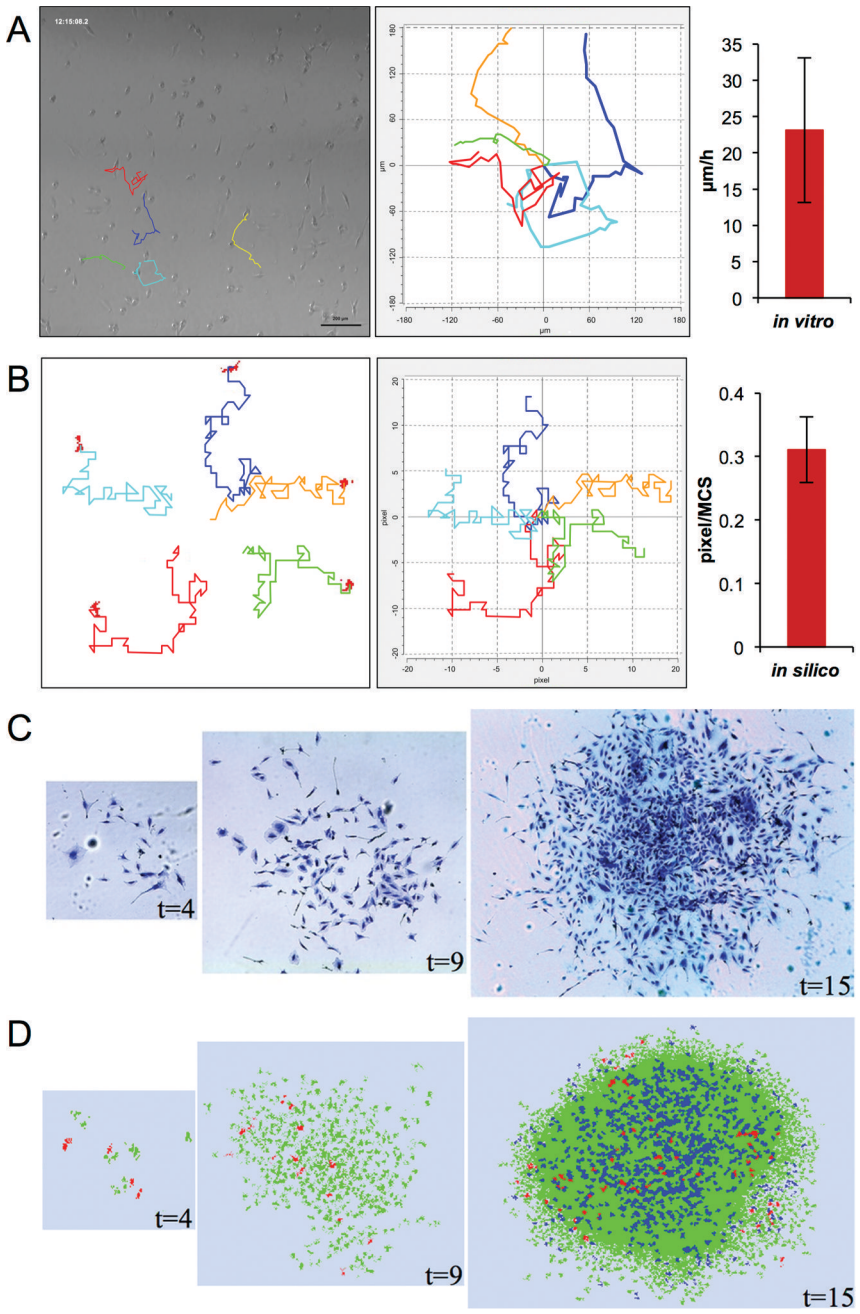

Figure 2.

Model parameterization. **(A)** Tracking of migrating U87-MG cells *in vitro* and re-plotted with a common origin (left panel). Average migration distance (right panel; mean ± s.d., n=24). **(B)** Tracking of migrating generalized cells *in silico* and re-plotted with a common origin (left panel). Average displacement distance (mean ± s.d., n=30). **(C)** *In vitro* growth of a U87-MG cell population at t=4, 9 and 15 days. **(D)** *In silico* growth of a parameterized cell population at t=4, 9 and 15 days. Color-coded are GSC (red), proliferating CC (green) and quiescent CC (blue). **(E)** Population expansion via self-metastases at t=15, 75 and 120 days. Circles are added to visualize separate population clusters. Arrows indicate the locations of GSCs. Parameters used in the present simulation include p_s=0.02, ρ_{max}=10. Figures in **(D)** and **(E)** labeled with star mark (*) are identical.

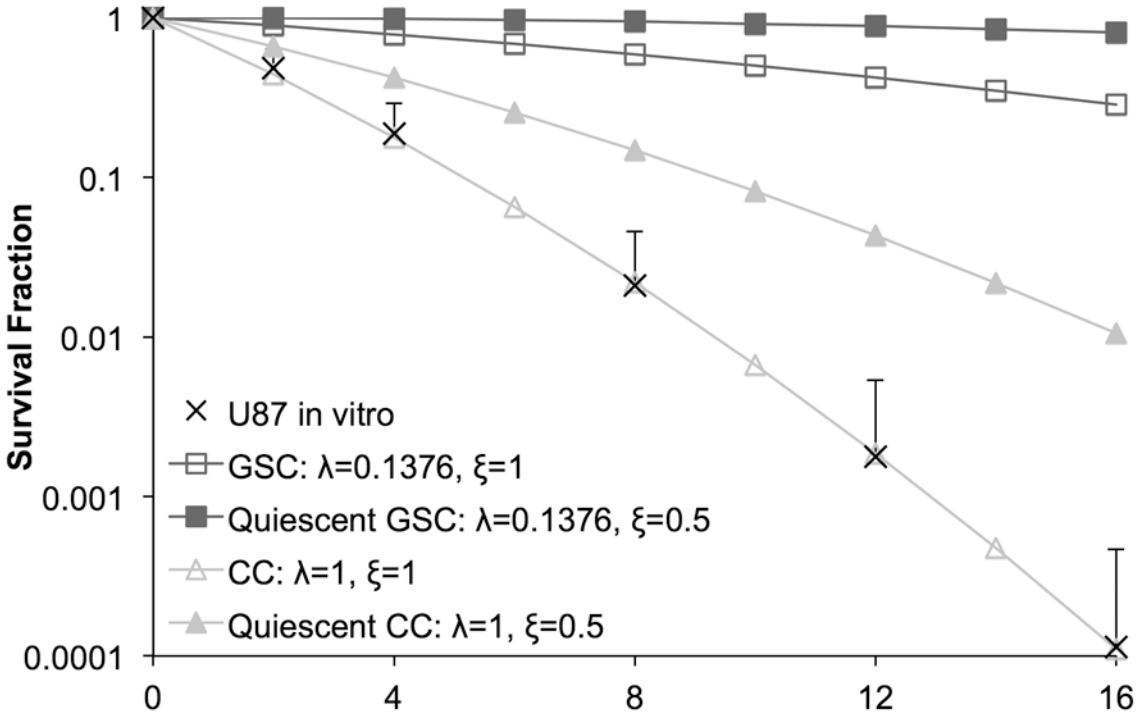

Figure 3.

Clonogenic survival fraction of U87-MG *in vitro* after single-doses of irradiation (mean + s.d., n=3) and unconstrained best-fit curve with α=0.3859 and β=0.01148. Survival curves plotted for estimated radioprotection factors of GSC (λ=0.1376) and quiescent CC/GSC (ξ=0.5).

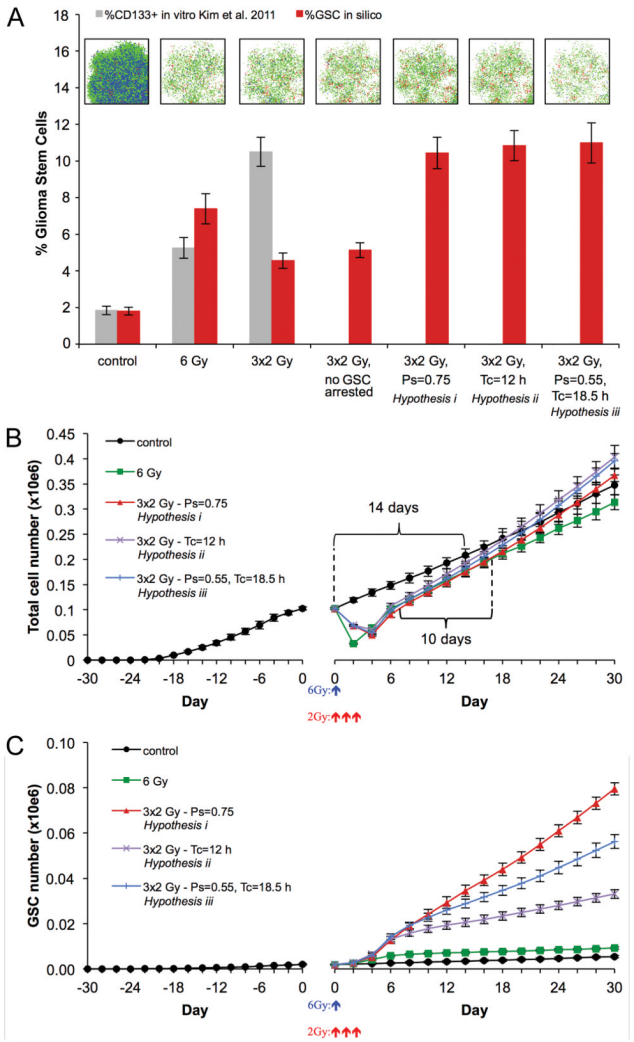

Figure 4.

(A) Enrichment of CD133$^+$ fraction *in vitro* (gray; means ± s.d., n=3) (22) and enrichment of GSC fraction *in silico* after irradiation for different GSC kinetics hypotheses (red; means ± s.d., n=5; see text for details). Representative *in silico* simulation snapshots are shown. Color-coded are GSC (red), proliferating CC (green) and quiescent CC (blue). Cell counts and simulation snapshots 48 hrs after irradiation. **(B)** Pre- and post-treatment total cell number evolution for different GSC kinetics hypotheses (means ± s.d., n=5). Treatment initiated at day 0. Curly brackets represent tumor population doubling times for control and irradiated tumors. **(C)** Pre- and post-treatment GSC number evolution for different GSC kinetics hypotheses (means ± s.d., n=5). Treatment initiated at day 0.

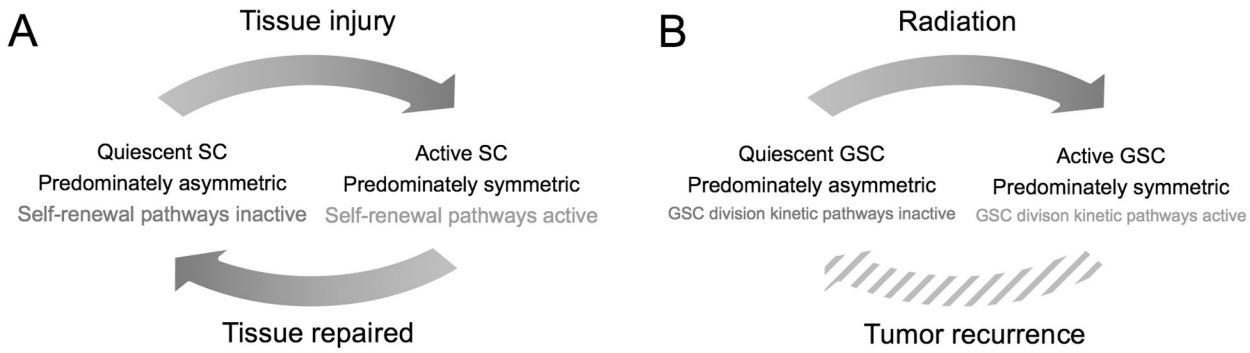

Figure 5.
(A) Normal stem cell (SC) response to tissue injury adapted from (34). **(B)** Proposed GSC response to fractionated irradiation exposure.

Table 1

Model parameters and values.

Parameter	Meaning	Value	Reference
r	Cell diameter	10 μm	*in vitro* U87-MG cell line
v	Cell migration speed	23.4 μm hr^{-1}	*in vitro* U87-MG cell line
T_c	Cell cycle time	25 hrs	*in vitro* U87-MG cell line
k	Cell growth rate	0.0213 pixel MCS^{-1}	*in vitro* U87-MG cell line
ρ_{max}	Non-stem cell proliferation capacity	10	assumed from (17)
p_s	GSC symmetric division rate	0.35	estimated using data from (22)
T_a	Cell cycle arrest time post IR	random in 0–16 hrs	*in vitro* U87-MG cell line (5)
α	Radiosensitivity of single-hit killing	0.3859	*in vitro* U87-MG cell line
β	Radiosensitivity of double-hit killing	0.01148	*in vitro* U87-MG cell line
λ_{GSC}	Radioprotection of GSCs	0.1376	estimated from *in vitro* U87-MG cell line and (11)
ξ	Radioprotection of non-cycling cells	0.5	(30,31)

Table 2

Comparison of tumor composition and growth rates after simulated IR schedules (means ± s.d., n=5).

	# of GSCs 48 hrs after IR at 10^5 cells	% of GSCs 48 hrs after IR at 10^5 cells	Post-IR population growth rate	# of total tumor cells 30 days after IR begins
Control	2137 ± 311	1.81% ± 0.21	0.0389	347,973 ± 19,788
6 Gy	2411 ± 318	7.4% ± 0.83	0.0445	313,866 ± 15,043
3×2 Gy, p_s=0.75 hypothesis (*i*)	5291 ± 707	10.44% ± 0.85	0.0527	367,254 ± 12,540
3×2 Gy, T_c=12 hrs hypothesis (*ii*)	6591 ± 801	10.84 %± 0.82	0.0535	403,629 ± 22,444
3×2 Gy, p_s=0.55, T_c=18.5 hrs hypothesis (*iii*)	5908 ± 851	10.99% ± 1.1	0.0539	395,517 ± 14,605